

Room-temperature ultrasensitive mass spectrometer via dynamical decouplingNan Zhao^{1,2,*} and Zhang-qi Yin^{3,†}¹*Beijing Computational Science Research Center, Beijing 100084, China*²*Synergetic Innovation Center of Quantum Information and Quantum Physics, University of Science and Technology of China, Hefei 230026, China*³*The Center for Quantum Information, Institute for Interdisciplinary Information Sciences, Tsinghua University, Beijing 100084, P. R. China*

(Received 25 November 2013; revised manuscript received 7 October 2014; published 23 October 2014)

We propose an ultrasensitive mass spectrometer based on a coupled quantum-bit-oscillator system. Under dynamical decoupling control of the quantum bit (qubit), the qubit coherence exhibits a comb structure in the time domain. The time-comb structure enables high-precision measurements of oscillator frequency, which can be used as an ultrasensitive mass spectrometer. We show that, in the ideal case, the sensitivity η of the proposed mass spectrometer has better performance at higher temperature and scales with the temperature T as $\eta \sim T^{-1/2}$. While taking into account qubit and oscillator decay, the optimal sensitivity reaches a universal value independent of environmental temperature T . The measurement sensitivity η also shows an improved dependence on the control-pulse number N as $\eta \sim N^{-3/2}$, in comparison with the $N^{-1/2}$ scaling in previous magnetometry studies. With the present technology on solid-state spin qubit and high-quality optomechanical system, our proposal is feasible to realize an ultrasensitive room-temperature mass spectrometer.

DOI: [10.1103/PhysRevA.90.042118](https://doi.org/10.1103/PhysRevA.90.042118)

PACS number(s): 06.20.-f, 37.10.Jk, 37.10.Vz, 42.50.Gy

I. INTRODUCTION

Single quantum objects, such as single atoms and single photons, have attracted more and more attentions in recent years. Novel applications, such as quantum information processing, triggered fast technique development in *isolating* single quantum objects from the noisy environment, precisely *controlling* their quantum states, and *hybridizing* different quantum systems. The technique development, in turn, provides opportunities of using single quantum objects to design more distinctive and more powerful tools in various research fields.

Detection of extremely weak signals, such as magnetic fields produced by single nuclei [1–5], and tiny mass of single molecules [6–11], has broad applications in chemistry and biology. In the past a few decades, detectors based on single quantum objects were designed, and their sensitivity was progressively improved. For example, quantum coherence and quantum lock-in amplification techniques are applied to single ions to improve the sensitivity of magnetometry [12]. By using mechanical cantilevers or well-controlled single spins, people are able to detect and resolve single spins of electrons [13] and nuclei [1–3]. For mass sensors, the minimum detectable mass was decreased from femtograms to yoctograms [7–11], reaching the single-proton limit.

In this paper, we propose an ultrasensitive measurement scheme based on a coupled quantum-bit-oscillator system. We show that, with many-pulse dynamical decoupling (DD) control [14] on the quantum bit (qubit) of the coupled system, the qubit coherence exhibits periodic sharp peaks, forming a *comb structure* in the time domain. The qubit coherence peaks are synchronized with the oscillator period, and the peak width

decreases when increasing the measurement *resource*; namely, the DD control pulse number. With this time-comb structure of the qubit coherence, tiny changes of the oscillator frequency, e.g., due to absorption of a single molecule onto a mechanical oscillator, can be monitored and precisely determined from the shift of the coherence peaks.

Two distinctive features allow our proposal to offer ultrahigh sensitivity and have outstanding performance at room temperature. First, the measurement sensitivity scales with the control-pulse number N as $\sim N^{-3/2}$, which is different in comparison to the $N^{-1/2}$ dependence in the magnetometry schemes using single qubits [15]. The improved scaling relation enables us reach high sensitivity with less measurement resource. Second, we show that the optimal sensitivity is *independent* of environmental temperature T , and fewer control pulses are required at high temperature to reach this optimal sensitivity. For most of the conventional sensing schemes, low-temperature (e.g., liquid helium temperature) is required, since measurement sensitivity is usually limited by thermal fluctuation proportional to $\sqrt{k_B T}$ (with Boltzmann constant k_B) [16,17]. The temperature-independent feature of the optimal sensitivity in our proposal allows novel applications at room temperature.

Recent technique development for solid-state qubit and mechanical oscillator provides the feasibility of our proposal. Single-spin qubits in solids, such as nitrogen-vacancy (NV) centers [18,19], have been demonstrated to be well isolated with long coherence times [20]. Meanwhile, the mechanical oscillators of micro- or nanosize have been experimentally fabricated and widely used in detecting weak signals [17,21]. In particular, the recent optomechanical systems [6,22,23], optically levitated particles [24–27], are believed to reach high quality factors, up to 10^{10} [28] or even higher, which enables such systems to detect novel quantum effects [29–31]. Here, we combine the advanced qubit and optomechanical systems and propose that hybrid systems such as an optically

*nzhaoc@csrc.ac.cn; <http://www.csrc.ac.cn/~nzhaoc>

†yinzhangqi@tsinghua.edu.cn

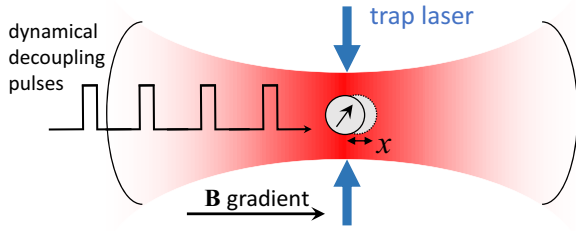


FIG. 1. (Color online) Schematic of the proposed mass spectrometer. A nanodiamond is trapped in a harmonic potential by counterpropagating laser beams. The nanodiamond (the gray circle) contains a NV center, which serves as a qubit. With a gradient magnetic field, the center-of-mass motion of the nanodiamond couples to the NV-center spin. Under DD control, the qubit coherence exhibits a time-comb structure, which can be used to measure the tiny change of the oscillation frequency (thus the mass change) of the nanodiamond.

levitated nanodiamond with a single NV center [32–34] can realize a high mass sensitivity of up to $10^{-22}\text{g}/\sqrt{\text{Hz}}$ at room temperature (see Fig. 1).

II. ULTRASENSITIVE MASS SPECTROMETER

A. Time-comb under dynamical decoupling

We consider a coupled qubit-oscillator model with the Hamiltonian [33–35]

$$H = \frac{1}{2}\omega_q\sigma_z + \omega_0 b^\dagger b + \frac{1}{2}\lambda\sigma_z(b^\dagger + b), \quad (1)$$

where ω_0 (ω_q) is the frequency of the harmonic oscillator (qubit), and λ is the coupling strength. The qubit is initially prepared in a superposition state $|\psi(0)\rangle_q = (|0\rangle + |1\rangle)/\sqrt{2}$, where $|0\rangle$ and $|1\rangle$ are the eigenbases of the qubit corresponding to $\sigma_z = -1$ and $+1$, respectively. The oscillator is initially in a thermal equilibrium state $\rho_b = Z^{-1} \exp(-\beta\omega_0 b^\dagger b)$ with the partition function $Z = \text{Tr}[\exp(-\beta\omega_0 b^\dagger b)]$ and the inverse effective oscillator temperature $\beta = 1/(k_B T)$, where k_B is the Boltzmann constant.

Since σ_z is a good quantum number in the Hamiltonian (1), we focus on the dynamics of the relative phase, or the quantum coherence [36] between qubit states $|0\rangle$ and $|1\rangle$ influenced by the oscillator. Under DD control of the qubit, which flips the qubit state by a train of π pulses applied at times \tilde{t}_j for $j = 1, 2, \dots, N$, the qubit coherence $L(t)$ is expressed as [37]

$$L(t) = \langle \mathcal{T}_c e^{-i \int_c \hat{X}(t') f(t') dt'} \rangle, \quad (2)$$

where the integral is performed on a time contour $c: 0 \rightarrow t \rightarrow 0$, \mathcal{T}_c is the contour-time-ordering operator, and $\hat{X}(t) = \lambda(b^\dagger e^{i\omega_0 t} + b e^{-i\omega_0 t})$ is proportional to the oscillator displacement in the interaction picture. The qubit flipping by DD control is described by the sign function $f(t)$, which toggles between $+1$ or -1 whenever a π pulse is applied.

The Gaussian-statistics nature of the harmonic oscillator allows the coherence in Eq. (2) to be exactly evaluated [35,38]. In particular, under the N -pulse Carr–Purcell–Meiboom–Gill (CPMG) sequence [with $N\pi$ pulses applied at $\tilde{t}_j =$

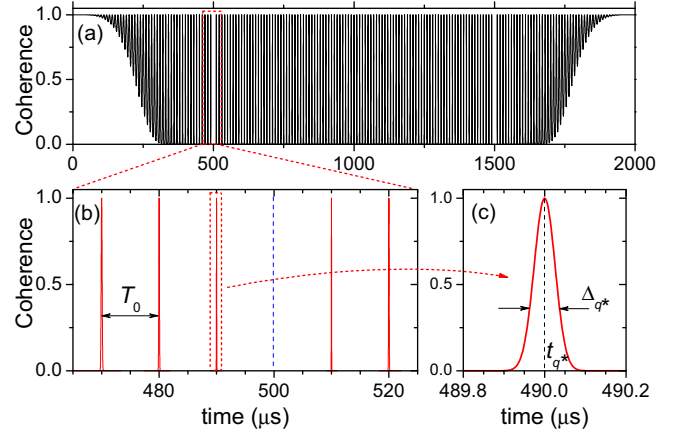


FIG. 2. (Color online) (a) The time-comb structure of qubit coherence under 100-pulse CPMG control. For $\omega_0 t \gg 1$, the comb period is synchronized with the oscillator period $T_0 = 2\pi/\omega_0$. (b) Closeup of the coherence peaks. A missing peak at $\omega_0 t = N\pi$ is indicated by the blue dashed line. The peak width is decreasing when it gets close to the missing one. (c) Closeup of the narrowest coherence peak, which is centered at t_{q^*} with width Δ_{q^*} (see text). The parameters used in this figure are oscillator frequency $\omega_0/(2\pi) = 100$ kHz, coupling strength $\lambda = 0.001\omega_0$, temperature $T = 10$ K, and 100-pulse CPMG control.

$(2j - 1)t/(2N)]$, the qubit coherence is $L(t) = \exp[-\chi(t)/2]$ with [35,38]

$$\begin{aligned} \chi(t) &= \int_0^\infty \frac{d\omega}{\pi} S(\omega) |F(\omega t)|^2 \\ &= \frac{4\tilde{\lambda}^2}{\omega_0^2} \left(\sec \frac{\omega_0 t}{2N} - 1 \right)^2 \sin^2 \frac{\omega_0 t}{2} \\ &\equiv \Gamma^2(t) \sin^2 \frac{\omega_0 t}{2}, \end{aligned} \quad (3)$$

where $S(\omega) = \tilde{\lambda}^2 \pi \delta(\omega - \omega_0)$ is the noise spectrum of the oscillator, $F(\omega t)$ is the Fourier transform of the modulation function $f(t)$, $\tilde{\lambda}^2 = \lambda^2(2n_{\text{th}} + 1)$, and $n_{\text{th}} \equiv [\exp(\beta\omega_0) - 1]^{-1}$ is the thermal occupation number of the oscillator. In the second line of Eq. (3), $\Gamma(t)$ is a slowly-varying-envelope function. Without loss of generality, we consider *even* pulse numbers $N \gg 1$ throughout the paper.

The qubit coherence exhibits novel dynamics with many-pulse DD, as shown in Fig. 2. In the short-time limit ($\omega_0 t \ll N\pi$), the qubit coherence is well protected (close to unity) by the DD control. With increasing time t , the qubit coherence become oscillatory. Furthermore, when $\Gamma(t) \gg 1$, the qubit enters a new regime where the coherence almost decays completely [$L(t) \approx 0$], *except* in the narrow intervals around the zero points of Eq. (3), i.e., $t_q = qT_0$ [for integer q and $q \neq (2k + 1)N/2$], where $T_0 = 2\pi/\omega_0$ is the oscillator period. In this regime, the qubit coherence forms a *comb structure*.

In the time-comb regime, the coherence shows sharp peaks in Gaussian shapes $L(t) \approx e^{-\gamma_q^2(t-t_q)^2/2}$ [see Fig. 2(c)]. The peak width decreases when t_q approaches an odd multiple of $NT_0/2$ [i.e., the divergence point of $\Gamma(t)$, indicated by the blue dashed line in Fig. 2(b)]. For a given control-pulse number N , the narrowest peak (for $q = q^* \equiv N/2 - 1$) appears at t_{q^*} and

with peak width Δ_{q^*}

$$t_{q^*} = \left(\frac{N}{2} - 1\right) T_0, \quad (4)$$

$$\Delta_{q^*} \equiv \frac{2\sqrt{2}}{\gamma_{q^*}} = \frac{T_0}{N\Lambda\sqrt{2n_{\text{th}} + 1}},$$

where $\Lambda = \lambda/\omega_0$ is the ratio of the coupling strength to the oscillator frequency. Notice that peak width is *inversely proportional* to the control pulse number N and the square root of the thermal excitation number n_{th} (for $n_{\text{th}} \gg 1$). Indeed, the peak-narrowing effect as increasing temperature (increasing n_{th}) was discovered for the case without DD control [39]. In the following, we show that increasing the pulse number N or the temperature T will improve the sensitivity.

B. Mass sensitivity

The unique time-comb structure can have broad applications in sensing weak signals. Here, we demonstrate the measurement principle through an example of measuring tiny mass change of the mechanical oscillator, e.g., due to absorption of single molecules. For an oscillator with frequency $\omega_0 = \sqrt{k/M}$ (for k and M being the spring constant and the mass, respectively), a small change δM of the mass M induces a change δL of the coherence $L(t)$ around the recovery peak. The relative mass uncertainty is

$$\frac{\delta M}{M} = \frac{2\delta\omega_0}{\omega_0} = \frac{1}{\gamma_{q^*}^2(t - t_{q^*})t_{q^*}} \frac{\delta L}{L} \approx \frac{1}{\gamma_{q^*}t_{q^*}} \frac{\delta L}{L}, \quad (5)$$

where we have chosen a proper measurement time t close to the peak time t_{q^*} so that $\gamma_{q^*}(t - t_{q^*}) \approx 1$.

We consider the case where the qubit coherence is obtained by averaging the output of N_{run} independent Bernoulli trials. In this case, the uncertainty δL comes from the shot noise in the measurement, i.e., $\delta L/L \approx N_{\text{run}}^{-1/2}$. For the total measurement time $T_{\text{tot}} = N_{\text{run}}t_{q^*}$, the mass sensitivity η_M , up to a constant of the order of unity, is

$$\eta_M \equiv \delta M \sqrt{T_{\text{tot}}} = \frac{M}{(2N)^{3/2} \Lambda \sqrt{k_B T/h}}, \quad (6)$$

where h is Planck's constant. Here we have assumed that $N \gg 1$ and $n_{\text{th}} \approx k_B T/(\hbar\omega_0) \gg 1$, which is the case for most practical mechanical oscillator systems.

Equation (6) reveals two interesting features of the qubit-oscillator-based mass spectrometer. First, the scaling relation of sensitivity to the pulse number N is different than what appears in magnetometry. In the case of using qubits for magnetometry under DD, the sensitivity scales with the control-pulse number as $\sim N^{-1/2}$ [15]. In our case, the peak-narrowing effect when increasing the pulse number N improves the scaling relation to $\sim N^{-3/2}$ [see Eq. (4)], which will help to more quickly achieve the optimal sensitivity. Physically, the peak-narrowing effect as increasing control-pulse number arises from the quantum interference between the *conditional* coherent evolution paths of the oscillator depending on the qubit states. In this sense, it is essentially a quantum effect.

Second, and more interestingly, the sensitivity is *inverse-linearly* dependent on the square root of temperature, i.e., $\eta_M \sim T^{-1/2}$. For traditional oscillator-based sensors, the

sensitivity is usually limited by thermal fluctuations of the oscillator displacement x , which are characterized by the root-mean-square amplitude $x_{\text{rms}} = \sqrt{k_B T/k}$. Weak signal corresponding to a displacement amplitude smaller than x_{rms} is hardly detected. High temperature would destroy the sensitivity and prevent the room-temperature applications. While in our measurement scheme, the measured quantity ω_0 does not directly couple to the oscillator displacement x and, thus, its uncertainty is independent of the position thermal fluctuations. Instead, the more thermal phonons at higher temperature cause stronger effective coupling between the qubit and oscillator [39], which improves the sensitivity.

III. DISCUSSION

A. Sensitivity limitations

Now we analyze the factors which limit the ideal sensitivity shown in Eq. (6). The qubit decoherence (including relaxation and dephasing) and the oscillation dissipation caused by the inevitable coupling to the environment are the two reasons which set the lower bound to the sensitivity.

The environmental fluctuation of the qubit, which causes qubit decoherence, prevents the perfect recovery of coherence shown in Fig. 2. With both the longitudinal relaxation process (or T_1 process) and transverse relaxation process (or T_2 process), the qubit suffers a background decoherence $L_{\text{bg}}(t)$ in addition to the oscillator-induced periodic revival peaks. Taking the solid-state spin qubit for example, the background decoherence can be modelled as $L_{\text{bg}}(t) = \exp[-t/T_1 - (t/T_2^{(N)})^3]$ [40]. The longitudinal decoherence, typically caused by phonon scattering, is a Markovian process (a simple exponential decay) and is hardly corrected by DD. The transverse decoherence, usually caused by spin baths, can be protected by DD with the decay time $T_2^{(N)}$ depending on the DD control-pulse number N as $T_2^{(N)} = T_2 N^{2/3}$ [40] (for T_2 being the coherence time for $N = 1$).

The background qubit decoherence $L_{\text{bg}}(t)$ reduces the height of the recover peaks. Consequently, the mass sensitivity is magnified by a factor of $L_{\text{bg}}^{-1}(t_{q^*})$. The balance between the $\sim N^{-3/2}$ sensitivity scaling and the background decoherence gives rise to an optimal pulse number to the sensitivity (see Fig. 3), similar to Ref. [15]. Qubits with long coherence time, like NV centers in diamond, can be chosen to suppress the background decoherence $L_{\text{bg}}(t)$ effect. At low temperature, the T_1 time can reach the order of seconds [41], and the T_2 time has been demonstrated to be \sim ms or even longer under DD control [42]. In this case, qubit decoherence becomes less important, and dissipation of mechanical oscillation is the dominant mechanism limiting the sensitivity.

The coupling to the environment of mechanical resonator causes broadening of the oscillator frequency. In Eq. (3), with the δ function in the noise spectrum $S(\omega)$ replaced by a Lorentzian spectrum with finite broadening $\kappa = \omega_0/Q$ [i.e., $S(\omega) = \tilde{\lambda}^2 \kappa / [(\omega - \omega_0)^2 + \kappa^2]$, with Q being the quality factor], the coherence cannot recover perfectly even though the central oscillation frequency hits the zero points of the filter function. The overlap between the wings of the Lorentzian spectrum and the nonzero region of the function $F(\omega t)$ causes the reduction of the height of the coherence recovery

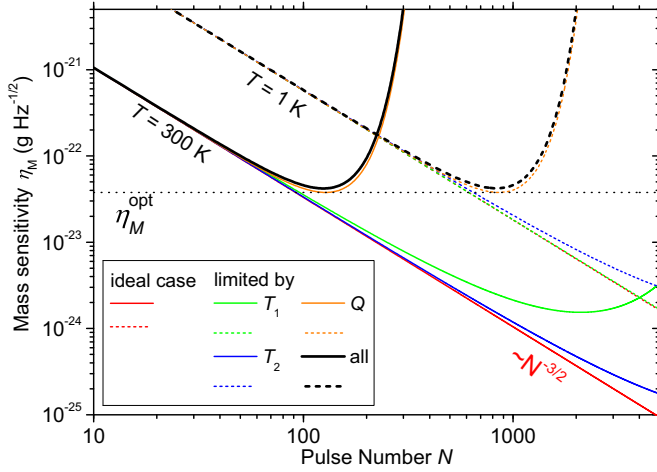


FIG. 3. (Color online) Mass sensitivity η_M as functions of DD control pulse number N . Solid curves are the sensitivity at room temperature $T = 300$ K, while dashed curves are the sensitivity at low temperature $T = 1$ K. The red curves are the ideal sensitivity according to Eq. (6), which scale as $\sim N^{-3/2}$. The curves in green, blue, and orange are the sensitivity taking into account the qubit T_1 decay (with $T_1 = 7$ ms), qubit T_2 decay (with $T_2 = 100$ μ s), and oscillator finite Q factor (with $Q = 10^9$), in turn. The thick black curves are the sensitivity with all the decay mechanisms included. The horizontal dotted line indicates the temperature-independent optimal sensitivity. The other parameters (ω_0 and λ) used in this figure are the same as those in Fig. 2.

peak [see Eq. (3)]. In the low- Q case (e.g., $Q \sim 10^2$ as demonstrated in Ref. [35]), the oscillator spectrum is too broad, so the coherence comb structure does not appear. In the case of $Q \gg N \gg 1$, the function $\chi(t)$ around the recovery time $t = t_{q^*}$ is calculated as $\chi(t) \approx \chi(t_{q^*}) + \gamma_{q^*}^2(t - t_{q^*})^2$ with $\chi(t_{q^*}) = 4\tilde{\lambda}^2 N^3 / (\omega_0^2 Q)$. Increasing the pulse number N reduces the recovery height. There exists an optimal control pulse number N_{opt} that minimizes the sensitivity in our scheme (see Fig. 3), which is estimated by considering $\chi(t_{q^*}) \approx 1$ and gives

$$N_{\text{opt}} \approx \frac{\omega_0}{2\lambda} \left(\frac{\hbar\lambda Q}{k_B T} \right)^{\frac{1}{3}}. \quad (7)$$

Substituting the optimal pulse number N_{opt} into Eq. (6), one obtains the optimal mass sensitivity of our proposal (up to a constant of the order of unity):

$$\eta_M^{\text{opt}} = \frac{M}{\sqrt{f_0 Q}}, \quad (8)$$

where $f_0 = \omega_0 / (2\pi)$. In our measurement scheme, the optimal sensitivity only relies on the properties of the oscillator (i.e., f_0 and Q) and is independent of the temperature T and of the qubit-oscillator coupling strength λ . In addition to the temperature-independent feature, we notice that, at higher temperature, less-controlled pulses are required to reach the optimal sensitivity according to Eq. (7) (see Fig. 3). In this sense, the proposed mass spectrometer has better performance at high temperature, in sharp contrast to conventional schemes where low temperature is necessary to reduce thermal fluctuations. The universal form of the optimal sensitivity in Eq. (8)

provides a simple guiding principle to design the system and to experimentally implement our proposal. The model and the sensitivity described in Eqs. (1)–(8), indeed, is quite general and can be realized in different types of systems [43,44]. In the following, we take the optically levitated nanodiamond with NV centers as an example to demonstrate the application.

B. Experimental feasibility

As discussed above, solid-state spin with long coherence time, like nitrogen-vacancies in diamond, serves as a good candidate for the qubit. The T_1 and T_2 decoherence has negligible effect on the sensitivity (see Fig. 3). Meanwhile, the coherent coupling between NV-center electron spin and mechanical motion has been demonstrated very recently [35] with a low- Q mechanical cantilever. Since a high quality factor Q of the mechanical oscillator is essential for ultimate sensitivity, we propose that the system of an optically levitated nanodiamond with a single NV center is a good candidate for realizing an ultrasensitive mass spectrometer, where the quality factor can reach $\sim 10^{10}$ or even higher.

In most cases, the mechanical quality Q of the oscillator is limited by the residual-gas-molecule collisions. In high or ultrahigh vacuum, the molecular mean-free path is larger than the diameter of the nanodiamond. The background gas induces a damping with rate $\gamma_g = (16/\pi)(P/vr\rho)$ [25], where P is the gas pressure and $v = \sqrt{8k_B T / (\pi m_a)}$ is the mean speed of the molecule with m_a being the mean mass of the molecule. In ultrahigh vacuum, the background-gas molecules are almost all hydrogen with mass $m_a = m_{\text{H}_2} = 3.3 \times 10^{-24}$ g. For a nanodiamond of diameter 50 nm and mass density $\rho = 3.5$ g/cm³, the damping rate is $\gamma_g / (2\pi) = 7.0 \times 10^{-6}$ Hz. With the oscillator frequency $\omega_0 / (2\pi) = 100$ kHz, the mechanical quality factor due gas-molecule collisions is $Q_g = \omega_0 / \gamma_g = 1.4 \times 10^{10}$. The strength of the gas-molecule collision effect is characterized by the average number $N_{\text{osc}}^{(\text{g})}$ of coherent oscillations before an oscillator energy quanta (a phonon) is created due to molecular collisions, i.e., $N_{\text{osc}}^{(\text{g})} = \omega_0 \tau_g / (2\pi)$ with $\tau_g = \hbar \omega_0 / (\gamma_g k_B T)$. A greater average oscillation number $N_{\text{osc}}^{(\text{g})}$ implies a weaker collision effect. At room temperature $T = 300$ K, the average oscillation number is $N_{\text{osc}}^{(\text{g})} \approx 37$.

As another possible damping mechanism, the photon-recoil effect is usually much weaker than molecular collisions. Photon scattering will heat the center-of-mass motion of the nanodiamond. We use the dipole approximation and calculate the photon-scattering rate when the nanodiamond is trapped in the Lamb-Dicke regime $\Delta x \ll 1/k$, where Δx is the position fluctuations of the nanodiamond, and k is the wave number of the trapping laser. The recoil heating rate for the phonon mode is

$$\gamma_{\text{sc}} = \frac{4\pi^2 \omega_0 \epsilon - 1}{5} \left(\frac{V}{\lambda^3} \right),$$

which depends on the ratio between the volume of the nanodiamond and the cube of the wavelength. Similar to $N_{\text{osc}}^{(\text{g})}$, the photon-recoil strength is characterized by the average oscillation numbers before a phonon is created by photon scattering: $N_{\text{osc}}^{(\text{sc})} = \omega_0 \tau_{\text{sc}} / (2\pi) \propto \lambda^3 / V$ with $\tau_{\text{sc}} = \gamma_{\text{sc}}^{-1}$. In

order to reduce the recoil heating effect, the laser wavelength should be much longer than the nanodiamond diameter. With a laser wavelength of $1.5 \mu\text{m}$ and the relative permittivity of diamond $\epsilon = 5.5$, the recoil heating rate $\gamma_{\text{sc}}/(2\pi) = 9.2 \text{ Hz}$, and $N_{\text{osc}}^{(\text{sc})} = 1.7 \times 10^3 \gg N_{\text{osc}}^{(\text{g})}$, which indicates that, for the condition discussed above ($P = 10^{-8} \text{ Torr}$, $\lambda = 1.5 \mu\text{m}$, $T = 300 \text{ K}$, and $Q \sim 10^{10}$), the photon-recoil effect is less important and the oscillator damping is dominated by collisions with background-gas molecules.

The mechanical quality factor Q can be further increased by decreasing the gas pressure. For example, if the background-gas pressure is reduced to $P' = 10^{-10} \text{ Torr}$, the damping rate becomes $\gamma'_{\text{g}}/(2\pi) = 7.0 \times 10^{-8} \text{ Hz}$, which corresponds to a quality factor as high as $Q'_{\text{g}} = 1.4 \times 10^{12}$. However, if the trapping-laser wavelength is kept unchanged ($\lambda = 1.5 \mu\text{m}$) and so is the recoil heating rate γ_{sc} , in this case, the coherent oscillation number due to collisions, $N_{\text{osc}}^{(\text{g})} = 3.7 \times 10^3$, becomes larger than that due to photon recoil, $N_{\text{osc}}^{(\text{sc})}$. In order to maintain the nanodiamond in the trap, the laser wavelength should be increased to $10 \mu\text{m}$. The recoil heating rate is decreased by more than two orders to $\gamma'_{\text{sc}}/(2\pi) = 0.03 \text{ Hz}$, corresponding to $N_{\text{osc}}^{(\text{sc})} = 5.0 \times 10^5$. In this case, the collision with gas molecules is still the dominating damping mechanism of the oscillator. We should note that the laser with $10 \mu\text{m}$ wavelength could melt the silica nanoparticles at high power, as discussed in Ref. [25]. However, the photon absorption rate of diamond is more than two orders lower than that of silica at the wavelength of $10 \mu\text{m}$ [34] and can afford much stronger laser power.

With the above discussions, we consider a nanodiamond of 50 nm in diameter (corresponding to a mass $M = 2.3 \times 10^{-16} \text{ g}$) which is optically trapped in a harmonic potential with center-of-mass (c.m.) oscillating frequency $f_0 = 100 \text{ kHz}$ (see Fig. 1). In a gradient magnetic field, the c.m. motion of the nanodiamond couples to the NV-center electron spin in the nanodiamond in the manner described in Eq. (1). With the magnetic-field gradient $G_m = 200 \text{ T/m}$, the coupling strength is $\sim 100 \text{ Hz}$. With the quality factor $Q = 10^9$, the system can reach a mass sensitivity of the order $\sim 10^{-22} \text{ g}/\sqrt{\text{Hz}}$. In practical experiments, the efficiency of the optical readout of the spin state of the NV center is limited by the spin-selective fluorescence contrast and the photon collection efficiency. This gives rise to a technique factor $1/C \approx 10^{-2} \sim 10^{-1}$, unfavourable for the sensitivity [45]. However, even though the technique factor may deteriorate, the sensitivity by one or two orders of magnitudes, the temperature-independent feature of our proposed system will be still attractive for a room-temperature sensor.

C. Comparison with oscillator under classical driving

Before concluding this paper, we compare our proposal with the classical mass-sensing scheme in Ref. [16]. In particular, we focus on the effects of thermal fluctuation on measurement sensitivity.

Thermal fluctuations are one of the most significant noise sources limiting the measurement sensitivity in the traditional scheme. In order to suppress the thermal-noise effect, one can drive the oscillator with an amplitude much larger than that

of the thermal fluctuations. As shown in Ref. [16], the mass sensitivity under classical driving is

$$\eta_M = \frac{\delta M}{\sqrt{\Delta f}} = 2M \sqrt{\frac{E_{\text{th}}}{E_{\text{dr}}} \frac{1}{Q\omega_0}}, \quad (9)$$

where Δf is the measurement bandwidth, and $E_{\text{th}} = k_B T$ and $E_{\text{dr}} = M\omega_0^2 x_{\text{dr}}^2$ are the thermal energy at temperature T and the driving energy corresponding to an amplitude x_{dr} , respectively. In order to suppress the thermal fluctuations ($E_{\text{dr}} > E_{\text{th}}$), the driving amplitude should be

$$x_{\text{dr}} > \sqrt{2n_{\text{th}}}\Delta x, \quad (10)$$

where $\Delta x = \sqrt{\hbar/(2M\omega_0)}$ is the zero-point-fluctuation amplitude. The large driving amplitude means injection of a large amount of energy into the system, which may limit the application of this technique if the oscillator cannot be driven so hard.

In contrast, making use of quantum coherence of the qubit, our proposal converts the thermal fluctuations into a useful measurement resource. Notice that, in Eq. (6) of the main text, the mass sensitivity is proportional to $T^{-1/2}$. Large thermal fluctuations at high temperature improve the sensitivity. This counterintuitive temperature dependence arises from the fact that, in our proposal, the oscillator-frequency change is monitored by the qubit coherence instead of by directly measuring the oscillator variables. In this sense, the quantum nature of the measurement principle causes the distinguishing feature in our proposal.

Furthermore, we consider the energy injected into the oscillator system during the mass-sensing process. The amplitude of the oscillator driven by the qubit-state-dependent force is

$$x(t) = \frac{2\lambda\Delta x}{\omega_0} \left(\sec \frac{\omega_0 t}{2N} - 1 \right) \sin \frac{\omega_0 t}{2}. \quad (11)$$

Using the parameters in Fig. 3 (i.e., the coupling strength $\lambda = 0.001\omega_0$ and the control-pulse number $N \sim 10^2$ to 10^3), the maximum amplitude

$$x_{\text{max}} = \frac{2N\lambda}{\omega_0} \Delta x \quad (12)$$

is much smaller than the thermal-fluctuation amplitude, i.e., $x_{\text{max}} \ll \sqrt{2n_{\text{th}}}\Delta x$. In other words, during the mass-sensing process, the oscillator state, which is perturbed by the qubit, only slightly deviates from the thermal-equilibrium state. Thus, our proposal provides a different measurement principle for mass sensing at low excitation power, which is complementary to the existing techniques in different practical situations.

IV. CONCLUSION

In this paper, we propose an ultrasensitive measurement scheme based on a coupled qubit-oscillator system. By using the many-pulse DD technique, the qubit coherence exhibits a time-comb structure, which enables the precise measurement of the oscillator frequency. The combination of advanced techniques on NV centers in diamond and optically levitated nanoparticles, which serve as long-lived qubits and high-

quality oscillators, respectively, makes the room-temperature ultrasensitive mass spectrometer ready to be realized.

ACKNOWLEDGMENTS

We thank Dr. L. Ge, Professor Y. Li, Professor W. Yang, Professor C.P. Sun, and Professor J. Twamley for fruitful discussions about the theoretical scheme, and Dr. T.C. Li, Dr.

F. Xue, Dr. Y. Tao, and Professor J. Wrachtrup for suggestions on the experimental feasibility. N.Z. is supported by NKBRP (973 Program) 2014CB848700 and NSFC No. 11374032 and No. 11121403. Z.Q.Y. is funded by the NBRPC (973 Program) 2011CBA00300 (2011CBA00302), and NNSFC 11105136, and 61033001.

-
- [1] N. Zhao, J. Honert, B. Schmid, M. Klas, J. Isoya, M. Markham, D. Twitchen, F. Jelezko, R.-B. Liu, H. Fedder, and J. Wrachtrup, *Nat. Nanotechnol.* **7**, 657 (2012).
- [2] S. Kolkowitz, Q. P. Unterreithmeier, S. D. Bennett, and M. D. Lukin, *Phys. Rev. Lett.* **109**, 137601 (2012).
- [3] T. H. Taminiau, J. J. T. Wagenaar, T. van der Sar, F. Jelezko, V. V. Dobrovitski, and R. Hanson, *Phys. Rev. Lett.* **109**, 137602 (2012).
- [4] H. J. Mamin, M. Kim, M. H. Sherwood, C. T. Rettner, K. Ohno, D. D. Awschalom, and D. Rugar, *Science* **339**, 557 (2013).
- [5] T. Staudacher, F. Shi, S. Pezzagna, J. Meijer, J. Du, C. A. Meriles, F. Reinhard, and J. Wrachtrup, *Science* **339**, 561 (2013).
- [6] J.-J. Li and K.-D. Zhu, *Phys. Rep.* **525**, 223 (2013).
- [7] N. V. Lavrik and P. G. Datskos, *Appl. Phys. Lett.* **82**, 2697 (2003).
- [8] M. Ganzhorn, S. Klyatskaya, M. Ruben, and W. Wernsdorfer, *Nat. Nanotechnol.* **8**, 165 (2013).
- [9] J. Chaste, A. Eichler, J. Moser, G. Ceballos, R. Rurali, and A. Bachtold, *Nat. Nanotechnol.* **7**, 301 (2012).
- [10] K. Jensen, K. Kim, and A. Zettl, *Nat. Nanotechnol.* **3**, 533 (2008).
- [11] A. K. Naik, M. S. Hanay, W. K. Hiebert, X. L. Feng, and M. L. Roukes, *Nat. Nanotechnol.* **4**, 445 (2009).
- [12] S. Kotler, N. Akerman, Y. Glickman, A. Keselman, and R. Ozeri, *Nature (London)* **473**, 61 (2011).
- [13] D. Rugar, R. Budakian, H. J. Mamin, and B. W. Chui, *Nature (London)* **430**, 329 (2004).
- [14] L. Viola, E. Knill, and S. Lloyd, *Phys. Rev. Lett.* **82**, 2417 (1999).
- [15] G. de Lange, D. Ristè, V. V. Dobrovitski, and R. Hanson, *Phys. Rev. Lett.* **106**, 080802 (2011).
- [16] K. Ekinici, Y. Yang, and M. Roukes, *J. Appl. Phys.* **95**, 2682 (2004).
- [17] J. Sidles, J. Garbini, K. Bruland, D. Rugar, O. Züger, S. Hoen, and C. Yannoni, *Rev. Mod. Phys.* **67**, 249 (1995).
- [18] A. Gruber, A. Drabenstedt, C. Tietz, L. Fleury, J. Wrachtrup, and C. von Borczyskowski, *Science* **276**, 2012 (1997).
- [19] J. Wrachtrup and F. Jelezko, *J. Phys.: Condens. Matter* **18**, S807 (2006).
- [20] G. Balasubramanian, P. Neumann, D. Twitchen, M. Markham, R. Kolesov, N. Mizuochi, J. Isoya, J. Achard, J. Beck, J. Tissler, V. Jacques, P. R. Hemmer, F. Jelezko, and J. Wrachtrup, *Nat. Mater.* **8**, 383 (2009).
- [21] A. N. Cleland, *Foundations of Nanomechanics: From Solid-State Theory to Device Applications* (Springer, Berlin, 2003).
- [22] F. Marquardt and S. Girvin, *Physics* **2**, 40 (2009).
- [23] M. Aspelmeyer, T. J. Kippenberg, and F. Marquardt, [arXiv:1303.0733](https://arxiv.org/abs/1303.0733).
- [24] O. Romero-Isart, M. L. Juan, R. Quidant, and J. I. Cirac, *New J. Phys.* **12**, 033015 (2010).
- [25] D. E. Chang, C. A. Regal, S. B. Papp, D. J. Wilson, J. Ye, O. Painter, H. J. Kimble, and P. Zoller, *Proc. Natl. Acad. Sci. USA* **107**, 1005 (2009).
- [26] T. Li, S. Kheifets, D. Medellin, and M. G. Raizen, *Science* **328**, 1673 (2010).
- [27] T. Li, S. Kheifets, and M. G. Raizen, *Nat. Phys.* **7**, 527 (2011).
- [28] Z.-Q. Yin, A. A. Geraci, and T. Li, *Int. J. Mod. Phys. B* **27**, 1330018 (2013).
- [29] A. A. Geraci, S. B. Papp, and J. Kitching, *Phys. Rev. Lett.* **105**, 101101 (2010).
- [30] A. Arvanitaki and A. A. Geraci, *Phys. Rev. Lett.* **110**, 071105 (2013).
- [31] Z.-Q. Yin, T. Li, and M. Feng, *Phys. Rev. A* **83**, 013816 (2011).
- [32] L. P. Neukirch, J. Gieseler, R. Quidant, L. Novotny, and A. Nick Vamivakas, *Opt. Lett.* **38**, 2976 (2013).
- [33] M. Scala, M. S. Kim, G. W. Morley, P. F. Barker, and S. Bose, *Phys. Rev. Lett.* **111**, 180403 (2013).
- [34] Z.-Q. Yin, T. Li, X. Zhang, and L. M. Duan, *Phys. Rev. A* **88**, 033614 (2013).
- [35] S. Kolkowitz, A. C. Bleszynski Jayich, Q. Unterreithmeier, S. D. Bennett, P. Rabl, J. G. E. Harris, and M. D. Lukin, *Science* **335**, 1603 (2012).
- [36] W. Yang, Z.-Y. Wang, and R.-B. Liu, *Front. Phys.* **6**, 2 (2011).
- [37] W. Yang and R.-B. Liu, *Phys. Rev. B* **78**, 085315 (2008).
- [38] N. Zhao, J. Hu, S. Ho, J. Wan, and R. Liu, *Nat. Nanotechnol.* **6**, 242 (2011).
- [39] C. P. Sun, X. X. Yi, S. R. Zhao, L. Zhang, and C. Wang, *Quantum Semiclassical Opt.* **9**, 119 (1997).
- [40] G. de Lange, Z. H. Wang, D. Riste, V. V. Dobrovitski, and R. Hanson, *Science* **330**, 60 (2010).
- [41] S. Takahashi, R. Hanson, J. van Tol, M. S. Sherwin, and D. D. Awschalom, *Phys. Rev. Lett.* **101**, 047601 (2008).
- [42] N. Bar-Gill, L. M. Pham, C. Belthangady, D. Le Sage, P. Cappellaro, J. R. Maze, M. D. Lukin, A. Yacoby, and R. Walsworth, *Nat. Commun.* **3**, 858 (2012).
- [43] D. M. Bell, C. R. Howder, R. C. Johnson, and S. L. Anderson, *ACS Nano* **8**, 2387 (2014).
- [44] S. Chakram, Y. S. Patil, L. Chang, and M. Vengalattore, *Phys. Rev. Lett.* **112**, 127201 (2014).
- [45] J. M. Taylor, P. Cappellaro, L. Childress, L. Jiang, D. Budker, P. R. Hemmer, A. Yacoby, R. Walsworth, and M. D. Lukin, *Nat. Phys.* **4**, 810 (2008).